Article

Interference Analysis for Vehicle-to-Vehicle Communications at 28 GHz

Omar A. Saraereh [1,†] , Ashraf Ali [1,†], Imran Khan [2,†] and Khaled Rabie [3,*,†]

1   Department of Electrical Engineering, Hashemite University, Zarqa 13133, Jordan; eloas2@hu.edu.jo (O.A.S.); ashraf@hu.edu.jo (A.A.)
2   Department of Electrical Engineering, University of Engineering and Technology Peshawar, P.O. Box 814, KPK, Pakistan; ikn.eup121@gmail.com
3   School of Electrical Engineering, Manchester Metropolitan University, Manchester M15 6BH, UK
*   Correspondence: k.rabie@mmu.ac.uk
†   These authors contributed equally to this work.

check for
updates

Abstract: High capacity and ultra-reliable vehicular communication are going to be important aspects of beyond 5G communication networks. However, the vehicular communication problem becomes complex at a large scale when vehicles are roaming on the road, while simultaneously communicating with each other. Moreover, at higher frequencies (like 28 GHz), the dynamics of vehicular communication completely shift towards unpredictability and low-reliability. These factors may result in high packet error and a large amount of interference, resulting in regular disruptions in communications. A thorough understanding of performance variations is the key to moving towards the next generation of vehicular networks. With this intent, this article aims to provide a comprehensive interference analysis, wherein the closed-form expressions of packet error probability (PEP) and ergodic capacity are derived. Using the expression of the PEP, diversity analysis is provided which unveils the impact of channel nonlinearities on the performance of interference-constrained vehicular networks. The insights provided here are expected to pave the way for reliable and high capacity vehicular communication networks.

Keywords: beyond 5G communications; high capacity; ultra-reliable; vehicle-to-vehicle (V2V) communications

1. Introduction

In recent years, vehicle-to-everything (V2X) communication has gained huge interest due to its ability to improve road safety and reduce the number of accidents [1]. The V2X communications generally refer to the exchange of information among different intelligent transportation systems (ITS) such as traffic safety, automated driving, and infotainment. It can be further subdivided into vehicle-to-vehicle (V2V), vehicle-to-infrastructure (V2I), vehicle-to-person (V2P) and vehicle-to-network (V2N) communication. Many efforts have been carried out to enable vehicular communication and the first of them was to allocate a dedicated 75 MHz spectrum by the United States Federal Communications Commission (FCC) [2] and 30 MHz by European Telecommunications Standards Institute (ETSI) [3] at 5.9 GHz.

Several communication technologies have already been developed to operate in 5.9 GHz band such as IEEE 802.11p [4] and Long-Term Evolution (LTE)-V2V [5]. However, the available spectrum is not enough for emerging V2X applications where high data rates are required, such as sharing cameras and Light Detection and Ranging(LIDARs) information [6–8]. Therefore, to offload traffic millimeter wave bands (mmWave), where more bandwidth is available, is being considered [6]. Many measurement campaigns have been carried out in the framework of some European Projects such as

DRIVE and PROMETHEUS [9] at mmWave. In this perspective, various requirements and use-cases are being considered with reference to both highway and urban applications [10]. In an urban scenario, vehicles can exchange information with the infrastructure and can collect data from other vehicles to generate information regarding traffic congestion and parking reservations, etc. [11].

The mmWave spectrum offers several advantages. First, large available channel bandwidth (e.g., 400 MHz per channel as defined in 5G New Radio (NR)) [12,13]. Second, due to smaller wavelengths at mmWave frequencies, it is possible to design a large number of antennas; therefore, directional beamforming is possible to boost the received signal power and reduce the impact of out-of-cell interference [14]. A large number of antennas enable the use of multiple-input multiple-output (MIMO) communication which further improves spectral efficiency. Overall higher network capacity is expected in the mm-wave band [15,16].

However, the mmWave band suffers from high path loss due to the higher order of frequencies which reduces the coverage area. Moreover, the Doppler shift is directly proportional to the carrier frequency and speed of the moving vehicle [17]. Doppler shift introduces inter-carrier-interference (ICI) in OFDM systems which could be potential limitations in enabling V2V communication [18]. In addition, signals at higher frequencies cannot penetrate from most solid materials such as walls. As a result, the movement of reflectors and obstacles, or even the orientation of UE can cause the channel to appear and disappear [19–21]. The wireless channel behavior at mmWave is totally different from the lower bands; hence, dedicated approaches are required to model the performance of a communication system.

1.1. Related Work

Experimental research platforms for using the mmWave band in the automotive industry have been developed since 1980. Lately, some studies have focused on the analysis of interference in mmWave vehicle communications [22–25]. In [22], a base station (BS) to vehicle communication at 60 GHz is modeled and outage probability is analyzed by taking into account the Rice channel model. The result shows that due to the movement of vehicles, the reflected signal from road infrastructure can be neglected as it has no impact. Furthermore, it is shown that high atmospheric absorption at 60 GHz leads to small cell sizes which, on one hand, increase the reuse factor, but on the other hand, enable frequent handovers. Nevertheless, it has been shown that communication can be established up to 100–200 m with a suitable value of outage probabilities.

The authors of [23] have considered interference from a nearby base-station during vehicle-to-infrastructure communication. It is shown that the dominating line-of-sight (LOS) interference, which determines the outage probability, is from BSs on the same street as the serving station, while the BSs on the cross street have insignificant effects in most cases. Furthermore, the results provided by the authors show that with the large intensity of BSs, the interference level rises and the network becomes interference-limited. Also, the coverage probability scales linearly with the street intensity. Therefore, the deployment of more BSs in an already dense Urban environment does not improve the coverage.

Interference from the sideline during mmWave V2V communication was measured by the authors of [24] for both highway and urban scenarios. Using these measurements, the authors estimated the signal-to-noise ratio (SNR) and performed capacity analysis for 79 and 300 GHz. The results indicate that the interference from the sidelines can be well approximated by 2D stochastic models. Besides, the interference level greatly depends on the radiation pattern and angle of arrival. The study presents a notable impact of interference from the sidelines on the link-layer performance of V2V communication systems.

A detailed framework to characterize the coverage and connectivity of a mmWave vehicular network deployed along a multi-lane highway is presented in [25]. The results show that stable connectivity requires both accurate alignments between vehicles and satisfactory signal quality. In sparse networks, it is observed that performance can be improved by considering narrower beams due to the beamforming gain. However, in dense networks, larger beams should be produced to

generate large connectivity regions that ensure robust alignment between vehicles. Overall, better connectivity and throughput performance are achieved by considering frequent beam alignments that enable endpoints to reduce the outage time.

Many investigations are carried out for V2X communication in 6 GHz bands such as [26–29]. These studies provide closed-form expressions for the achievable throughput and analyze coverage for V2V communication in various scenarios. However, the propagation characteristics at 5.9 GHz are completely different from those of mmWave communication. Also, communication in a conventional vehicular system is omnidirectional although beamforming is possible after the link has been established. Therefore, these solutions cannot be applied to mmWave scenarios, where highly directional transmission schemes are required.

Most of the above studies consider frequencies above a 60 GHz band. However, significant signal attenuation can be experienced at these frequency ranges. A more suitable approach is to use a 28 GHz frequency range where the atmospheric attenuation is identical to the cellular band [30]. The measurement campaign carried out in a dense urban scenario [30] shows that consistent coverage can be achieved with a cell radius of 200 m. Furthermore, coverage and capacity analysis in [31] for cellular communication at 28 GHz shows huge potential in terms of coverage and capacity. Additionally, the 28 GHz band, with spectrum allocation of more than 1 GHz of bandwidth, is currently available for use [30]. Therefore, in this paper, communication characteristics are analyzed in 28 GHz for V2V communication.

1.2. Motivation and Contributions

Though significant work has been done on the optimization and performance analysis of sub-6-GHz vehicular networks, there is a lack of understanding regarding the communication characteristics of vehicular networks at higher frequencies. Especially, it is important to characterize the inter-vehicle (V2V) communications for both LOS and non-LOS conditions. Since real-time simulations require a significant amount of computation resources, the closed-form expressions of different performance metrics of vehicular networks can help evaluate the performance of such networks. In addition, these expressions can help provide more insights regarding system performance in different states.

Motivated by the above-stated positive considerations, we perform packet error probability (PEP) analysis of V2V communications under co-channel interference at 28 GHz. Besides this, we also provide an analytical expression of the ergodic capacity of vehicular networks at 28 GHz. Using this expression, a diversity analysis has also been performed which shows that the probability of receiving an erroneous packet depends on the number of multipath clusters and channel non-linearity in V2V communications. These expressions have been validated by performing extensive Monte Carlo simulations. The results indicate that the provided analytical expressions closely follow the simulation results.

1.3. Organization

The remainder of the paper is organized as follows. Section 2 presents the details of the system model. In Section 3, analytical expression of PEP is provided with derivations. Section 4 provides the details of derivations of ergodic capacity. In Section 5 simulation results and their discussion is given. Finally, Section 6 concludes the work and provides some future research directions.

2. System Model

A typical V2V communication scenario, for a two-lane highway, is considered like [32]. As shown in Figure 1, each lane constitutes a cluster of vehicles $\mathcal{V} = \{V_j | j = 1, 2, 3...N\}$, wherein each vehicle is equipped with a single antenna. In each cluster, there are $N - 1$ member vehicles besides the cluster head (CH) which assists the member vehicles to forward their messages across the network. It is worth highlighting that this paper focuses on the performance analysis of V2V communications at

28 GHz. Therefore, we assume that the roadside unit (RSU) selects a CH based on some preset criteria. The selection criteria of the CH is beyond the scope of this work. Besides, a block fading model has been considered where the wireless link changes randomly from a one-time slot to another but remains unchanged within a particular time slot [33]. Due to usage of the same frequencies, the transmission in one of the clusters causes interference in the adjacent cluster. In this case, the received signal at the CH can be written as

$$\sqrt{P_c}|h_c|^2 s_c + \sqrt{P_i}|h_i|s_i + n, \tag{1}$$

where P_c is the power of the main signal, h_c is the channel gain of the channel between a member vehicle and the CH, s_c is the symbol transmitted by the member vehicle of the main cluster, P_i is the power of the interfering signal, h_i is the channel gain of the channel between a member vehicle of the interfering cluster and the CH, s_i is the symbol transmitted by the member vehicle of the interfering cluster, and n is the additive white Gaussian noise (AWGN) with zero mean and N_0 variance. The signal-to-noise ratio at the received signal is written as $\frac{\lambda_c}{\lambda_i + 1}$, where

$$\lambda_c = \frac{P_c|h_c|^2}{N_0} \tag{2}$$

and

$$\lambda_i = \frac{P_i|h_i|^2}{N_0}. \tag{3}$$

All the links are considered to follow $\alpha - \eta - \kappa - \mu$ distribution [34]. In order to model LOS and non-LOS conditions at 28 GHz, this composite fading distribution has shown significant promise [34]. This distribution is defined by six main parameters including $\alpha, \eta, \kappa, \mu, p, q$. The details of these parameters along with their individual significance can be easily found in [34]. Primarily, these parameters characterize the effect of nonliterary and multipath components of the wireless channel. In this work, generalized expressions are investigated, however, it is worth pointing out that different values of fading parameters may refer to different channel conditions in mmWave band. In particular, when $\alpha = 2.2, \eta = 73, \kappa = 5.7, \mu = 1.01, p = 1.05, q = 1$ the distribution resembles to LOS outdoor channel, whereas, when $\alpha = 2.545, \eta = 0.006, \kappa = 2.5, \mu = 1.98, p = 1.5, q = 1.05$ the distribution follows non-LOS outdoor channel conditions at 28 GHz [34]. The probability density function (PDF) of envelop of $\alpha - \eta - \kappa - \mu$ distribution is given as [35]

$$f_R(\rho) = \frac{\alpha \rho^{(\alpha\mu - 1)} \exp\left(-\frac{\rho^\alpha}{2}\right)}{2^\mu \Gamma(\mu)} \sum_{k=0}^{\infty} \frac{k! c_k}{(\mu)_k} L_k^{(\mu-1)}(2\rho^\alpha), \tag{4}$$

where $\Gamma(.)$ is the well-known gamma-function, $(.)_k$ is the Pochhammer symbol, and $L_s^t(.)$ is the Laguerre polynomial [36]. Moreover, the value of c_k is calculated using ([35] (15), (30), (31)). Consequently, the CDF of the of the envelop is given as [35]

$$F_R(\rho) = \sum_{k=0}^{\infty} \frac{k! m_k}{(\mu+1)_k} L_k^\mu \left(\frac{2(\mu+1)\rho^\alpha}{\mu}\right) \times \frac{\rho^{(\alpha\mu)} \exp\left(-\frac{\rho^\alpha}{2}\right)}{2^{(\mu+1)} \Gamma(\mu+1)}, \tag{5}$$

where m_k can be obtained with the help of $\alpha, \eta, \kappa, \mu, p, q$ ([35] (16), (33), (34)). Now, using (4) and $\lambda_x = \frac{P_x|h_x|^2}{N_0}$, where $x \in \{c, i\}$, we get the expression for the PDF of instantaneous SNR of x

$$
f_{\lambda_x}(\lambda) = \frac{\alpha_x \lambda^{\left(\frac{\alpha_x \mu_x}{2} - 1\right)}}{2^{(\mu_x+1)} \Gamma(\mu_x) (\bar{\lambda}_x)^{\left(\frac{\alpha_x \mu_x}{2}\right)}} \exp\left(-\frac{\lambda^{\frac{\alpha_x}{2}}}{2(\bar{\lambda}_x)^{\frac{\alpha_x}{2}}}\right)
$$
$$
\times \sum_{k=0}^{\infty} \frac{k! c_{k,x}}{(\mu_x)_k} L_k^{(\mu_x-1)}\left(2\left(\frac{\lambda}{\bar{\lambda}_x}\right)^{\frac{\alpha_x}{2}}\right). \tag{6}
$$

Similarly, the CDF of SNR is given by using λ_x and (5) as

$$
F_{\lambda_x}(\lambda) = \frac{\left(\frac{\lambda}{\bar{\lambda}_x}\right)^{\left(\frac{\alpha_x \mu_x}{2}\right)} \exp\left(-\frac{\lambda^{\left(\frac{\alpha_x}{2}\right)}}{2(\bar{\lambda}_x)^{\left(\frac{\alpha_x}{2}\right)}}\right)}{2^{(\mu_x+1)} \Gamma(\mu_x+1)} \sum_{k=0}^{\infty} \frac{k! m_{k,x}}{(\mu_x+1)_k}
$$
$$
\times L_k^{\mu_x}\left\{\frac{2(\mu_x+1)}{\mu_x}\left(\frac{\lambda}{\bar{\lambda}_x}\right)^{\frac{\alpha_x}{2}}\right\}. \tag{7}
$$

In (6) and (7), $\bar{\lambda}_x = \frac{P_x}{N_0}$ denotes the mean value of the channel gain of the corresponding link.
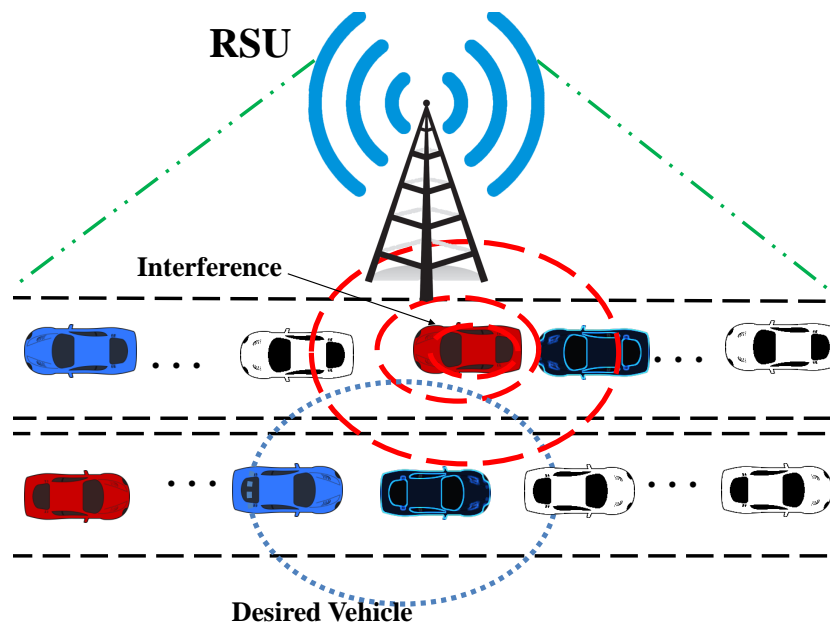

Figure 1. System model for V2V communications.

3. Analysis of PEP

In the following, we derive the expression of PEP for aforementioned system model. We consider that a packet prior transmission is divided into M blocks, where the value of M depends on the speed of transmitting and receiving vehicles. Specifically, it can be written as $M = \frac{\omega}{T_c \log(1+\psi)}$ [32], where ω is the packet size, T_c refers to the duration of the coherence period which is a function of Doppler shift, and ψ is the required data rate. Assuming ideal coding and modulation in vehicular networks, the PEP is based on the outage effect of the wireless channel [32]. Thus, the PEP can be written as

$$
P_e = 1 - (1 - P_{err})^M, \tag{8}
$$

where

$$P_{err} = \Pr\{\log(1 + \frac{\lambda_c}{\lambda_i + 1}) \leq \psi\} = \Pr\{\lambda_c \leq (2^\psi - 1)(1 + \lambda_i)\} = \int_0^\infty \int_0^{(2^\psi - 1)(1+\lambda_i)} f_{\lambda_c}(\lambda_c) f_{\lambda_i}(\lambda_i) d\lambda_c d\lambda_i. \quad (9)$$

By replacing (6), applying variable transform and using identities ([36] (3.381), (8.970)), P_{err} can be simplified as

$$
\begin{aligned}
P_{err} = & \frac{\alpha_i 2^{-(\mu_i + \mu_c + 2)} \left(\bar{\lambda}_c\right)^{\left(-\frac{\alpha_c \mu_c}{2}\right)}}{\Gamma(\mu_i) \Gamma(\mu_c) \left(\bar{\lambda}_i\right)^{\left(\frac{\alpha_i \mu_i}{2}\right)}} \sum_{n=0}^\infty \frac{n! c_{n,i}}{(\mu_i)_n} \sum_{s=0}^n \frac{(-1)^s 2^s}{s! (\lambda_i)^{\left(\frac{\alpha_i s}{2}\right)}} \\
& \times \binom{n + \mu_i - 1}{n - s} \sum_{k=0}^\infty \frac{k! c_{k,c}}{(\mu_c)_k} \sum_{r=0}^k \frac{(-1)^r 2^{(r+1)}}{r! (\bar{\lambda}_c)^{\left(\frac{\alpha_c r}{2}\right)}} \binom{k + \mu_c - 1}{k - r} \\
& \times \left(2 \left(\bar{\lambda}_c\right)^{\left(\frac{\alpha_c}{2}\right)}\right)^{(\mu_c + r)} \times \int_0^\infty \lambda_i^{\left(\frac{\alpha_i(\mu_i + s)}{2} - 1\right)} \exp\left(-\frac{\lambda_i^{\left(\frac{\alpha_i}{2}\right)}}{2\bar{\lambda}_i^{\left(\frac{\alpha_i}{2}\right)}}\right) \\
& \times \gamma\left(\mu_c + r, \frac{\{(2^\psi - 1)(1 + \lambda_i)\}^{\frac{\alpha_c}{2}}}{2(\bar{\lambda}_c)^{\left(\frac{\alpha_c}{2}\right)}}\right) d\lambda_i,
\end{aligned}
\quad (10)
$$

where $\gamma(.)$ denotes the incomplete gamma function [36]. In order to further simplify the above expression, we first apply the identity ([36] (8.354)). After performing some mathematical manipulations and using ([37] (2.2)), we get P_{err} as

$$
\begin{aligned}
P_{err} = & \sum_{n=0}^\infty \frac{n! c_{n,i}}{(\mu_i)_n} \times \sum_{s=0}^n \frac{(-1)^s 2^s \binom{n + \mu_i - 1}{n - s}}{s! (\bar{\lambda}_i)^{\left(\frac{\alpha_i s}{2}\right)} \left(\frac{2^\psi - 1}{2^\psi - 2}\right)^{\left(\frac{\alpha_i(\mu_i + s)}{2}\right)}} \sum_{k=0}^\infty \frac{k! c_{k,c}}{(\mu_c)_k} \\
& \times \sum_{r=0}^k (-1)^r 2^{(r+1)} \binom{k + \mu_c - 1}{k - r} \frac{2^{-(\mu_i + \mu_c + \alpha_i + 1)} \left(\lambda_c\right)^{\left(-\frac{\alpha_c \mu_c}{2}\right)}}{\pi^{(\alpha_i - 0.5)} \Gamma(\mu_i) \Gamma(\mu_c) \left(\bar{\lambda}_i\right)^{\left(\frac{\alpha_i \mu_i}{2}\right)}} \\
& \times \sum_{l=0}^\infty \left(\frac{2^\psi - 2}{\alpha_i}\right)^{\left(\frac{\alpha_c(\mu_c + r + l)}{2}\right)} \times \frac{(-1)^l \left(2\bar{\lambda}_c^{\left(\frac{\alpha_c}{2}\right)}\right)^{-l}}{l! (\mu_c + r + l) \Gamma\left(-\frac{\alpha_c(\mu_c + r + l)}{2}\right)} \\
& \times G_{\alpha_i, 2 + \alpha_i}^{2 + \alpha_i, \alpha_i} \left(\frac{1}{16} \left(\frac{2^\psi - 2}{2^\psi \bar{\lambda}_i - \bar{\lambda}_i}\right) \middle| \begin{array}{c} \Xi(\alpha_i, \xi_1) \\ \Xi(2, 0), \Xi(\alpha_i, \xi_2) \end{array}\right),
\end{aligned}
\quad (11)
$$

where

$$\Xi(y, z) = \frac{z}{y} + \frac{z + 1}{y} + ... \frac{z + y - 1}{y}, \quad (12)$$

$$\xi_1 = 1 - \frac{\alpha_i(\mu_i + s)}{2}, \quad (13)$$

and

$$\xi_2 = -\frac{\alpha_i(\mu_i + s)}{2} - \frac{\alpha_i(\mu_c + r + l)}{2}. \quad (14)$$

Using the above closed-form expression, we can perform the diversity analysis of the system. For a specific value of $\bar{\lambda}_i$, the diversity gain can be written as

$$\mathcal{D} = -\lim_{\bar{\lambda}_c \to \infty} \frac{\log(P_{err})}{\log(\bar{\lambda}_c)}. \tag{15}$$

From (11), it can be observed that in a high SNR region, the dominant value of $\bar{\lambda}_c$ will correspond to the largest value of its exponent. Thus, for a specific value of M at high SNR, we note that the curve of PEP will fall with the slope of $0.5\alpha_c\mu_c$. This also shows that the PEP, at high SNR, depends on the total number of multipath clusters and the channel non-linearity.

4. Ergodic Capacity

We now provide the ergodic capacity expression for the above mentioned scenario. The ergodic capacity can be defined as

$$C_{erg} \equiv \int_0^\infty \int_0^\infty \log\left(\frac{\lambda_c}{\lambda_i}\right) f_{\lambda_c,\lambda_i}(\lambda_c, \lambda_i) \, d\lambda_c d\lambda_i = F_1 + F_2 - F_3, \tag{16}$$

where $F_1 = \int_0^\infty \log(\lambda_c) \times f_{\lambda_c}(\lambda_c) \times F_{\lambda_i}(\lambda_c) \, d\lambda_c$, $F_2 = \int_0^\infty \log(\lambda_i) \times f_{\lambda_i}(\lambda_i) F_{\lambda_c}(\lambda_i) \, d\lambda_i$, and $F_3 = \int_0^\infty \log(\lambda_i) f_{\lambda_i}(\lambda_i) d\lambda_i$. Using the identities of Meijer G function ([37] (8.4.3), (8.4.6)) and then applying ([37] (8.3.1)), we obtain

$$F_1 = \frac{2^{-(\mu_c+\mu_i+2)}\alpha_c (\bar{\lambda}_c)^{\left(-\frac{\alpha_c\mu_c}{2}\right)}}{\Gamma(\mu_c)\Gamma(\mu_i+1)(\bar{\lambda}_i)^{\left(\frac{\alpha_i\mu_i}{2}\right)}} \times \sum_{k=0}^\infty \frac{k! c_{k,B}}{(\mu_c)_k} \times \sum_{n=0}^\infty \frac{n! m_{n,i}}{(\mu_i+1)_n}$$

$$\times \sum_{r=0}^k (-1)^r 2^r \binom{k+\mu_c-1}{k-r} \sum_{s=0}^n \frac{(-1)^s 2^s (\mu_i+1)^s \binom{n+\mu_i}{n-s}}{s! \mu_i^s (\bar{\lambda}_i)^{\left(\frac{\alpha_i s}{2}\right)}}$$

$$\times H_{1,0:0,1:2,2}^{0,1:1,0:1,2}\left(1-\left(\mu_c+r+\frac{\alpha_i(\mu_i+s)}{\alpha_c}\right)\middle|\begin{array}{c}-\\-\end{array}\middle|\begin{array}{c}(1,1),(1,1)\\(0,1)\end{array}\middle|\begin{array}{c}(1,1),(0,1)\end{array}\xi_3,\xi_4\right)$$

$$\times \left(2(\bar{\lambda}_c)^{\frac{\alpha_c}{2}}\right)^{\left(\frac{\alpha_i(\mu_i+s)}{\alpha_c}+\mu_c+r\right)}, \tag{17}$$

where $\xi_3 = \frac{\left(2(\bar{\lambda}_c)^{\frac{\alpha_c}{2}}\right)^{\frac{\alpha_i}{\alpha_c}}}{2(\lambda_i)^{\frac{\alpha_i}{2}}}$, $\xi_4 = 2^{\frac{2}{\alpha_c}}\bar{\lambda}_c$, and $H_{a,b:c,d:e,f}^{g,h:i,j:k,l}(.)$ is the EGBFHF function [38]. The EGBFHF function can be easily implemented in standard computation softwares like Mathematica. Due to limitation of space, we omit the computation of F_2 which can obtained by following the steps of F_1. For F_2, we get the expression like F_1, however, the values of α_c, μ_c and $\bar{\lambda}_c$ in F_1 are replaced by α_i, μ_i and $\bar{\lambda}_i$ and vice versa. In order to get F_3, we use ([37] (8.4.3), (8.4.6)) along with identity ([36] (8.970)) which finally yields

$$F_3 = \sum_{k=0}^\infty \sum_{l=0}^k \frac{(-1)^l 2^{(l-\mu_i-0.5)} k! c_{k,i} \binom{k+\mu_i-1}{k-l}}{(2\pi)^{(\alpha_i-0.5)} l! \Gamma(\mu_i)(\mu_i)_k (\bar{\lambda}_i)^{\left(\frac{\alpha_i(\mu_i+l)}{2}\right)}}$$

$$\times G_{2\alpha_i,2+2\alpha_i}^{2+2\alpha_i,2\alpha_i}\left(\frac{1}{16(\bar{\lambda}_i)^{\alpha_i}}\middle|\begin{array}{c}\Xi(\alpha_i,\xi_5),\Xi(\alpha_i,\xi_6)\\\Xi(2,0),\Xi(\alpha_i,\xi_7),\Xi(\alpha_i,\xi_8)\end{array}\right), \tag{18}$$

where $\xi_5 = -\frac{\alpha_i(\mu_i+l)}{2}$, $\xi_6 = 1 - \frac{\alpha_i(\mu_i+l)}{2}$, $\xi_7 = -\frac{\alpha_i(\mu_i+l)}{2}$, and $\xi_8 = 1 - \frac{\alpha_i(\mu_i+l)}{2}$. By straightforward substitution of F_1, F_2 and F_3 in (16), we can obtain the expression of ergodic capacity.

5. Results and Discussion

In this section, we provide simulation results along with the relevant discussion. The link-level simulations were performed in MATLAB to validate the expressions. Moreover, we have performed Monte Carlo simulations for both LOS and non-LOS conditions. We have fixed the value of $\alpha, \eta, \kappa, \mu, p, q$ throughout the simulations. Specifically, the value of $\alpha = 2.2, \eta = 73, \kappa = 5.7, \mu = 1.01, p = 1.05, q = 1$ for LOS outdoor channel, whereas, for non-LOS outdoor channel $\alpha = 2.545, \eta = 0.006, \kappa = 2.5, \mu = 1.98, p = 1.5, q = 1.05$. Besides this, although there are infinite summations in P_e and C_{erg}, these summations easily converge for small values of k, n and l. Furthermore, the values of other simulation parameters are $k = 10$, $n = 10$, $l = 15$, and $\psi = 2$ bits/s/Hz.

Figure 2 shows P_e against increasing values of $\bar{\lambda}_c$. It can be seen that the probability of receiving erroneous packets decreases when $\bar{\lambda}_c$ increases, whereas, it increases with an increase in $\bar{\lambda}_i$. Moreover, the PEP is higher for non-LOS conditions as compared to the LOS communication scenario which shows the impact of blockage at higher frequencies. Due to these blockages, the signal cannot penetrate through the object which results in high PEP for non-LOS conditions. The increasing values of M also increase the P_e which shows that smaller coherence time increases the probability of receiving erroneous packets.
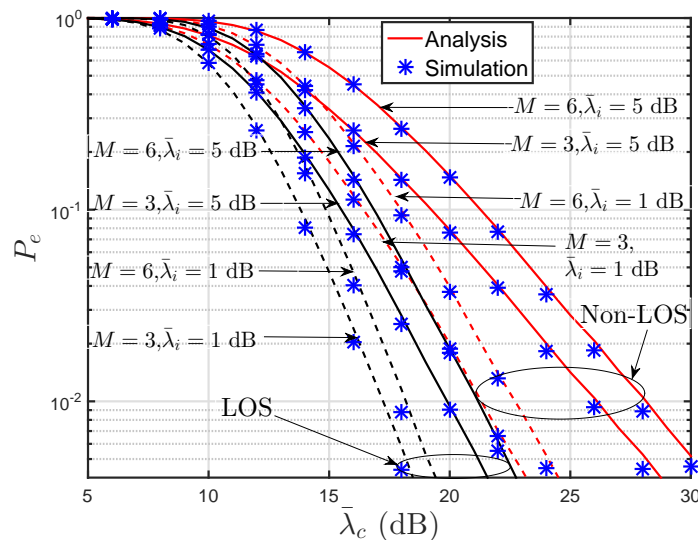

Figure 2. Probability of receiving erroneous packets versus $\bar{\lambda}_c$.

In Figure 3, ergodic capacity curves are plotted as a function of $\bar{\lambda}_c$. Here, it can be noted that the analytical curves closely corroborate with the simulation results. Additionally, an increase in the $\bar{\lambda}_c$ increases the overall ergodic capacity for both LOS and non-LOS conditions. The smallest ergodic capacity is achieved when non-LOS communication takes place under a high value of $\bar{\lambda}_i$. Furthermore, the gap between the non-LOS and LOS curves increases at higher values of $\bar{\lambda}_c$. This shows the signal power greatly impacts of LOS and non-LOS conditions for vehicular networks.
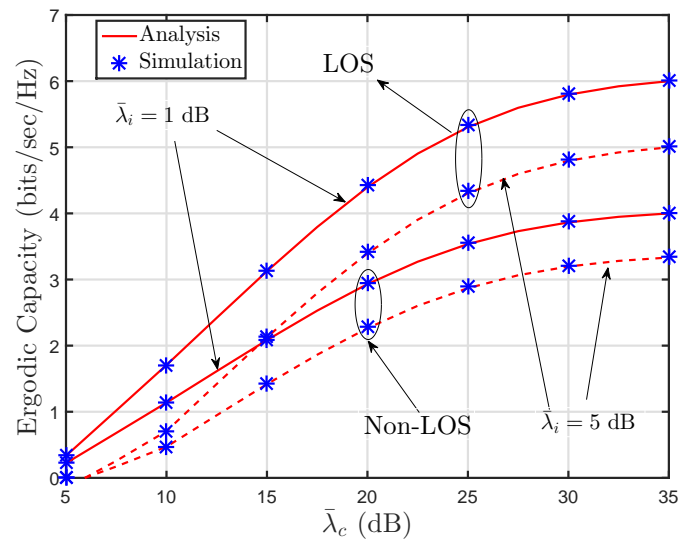
Figure 3. Ergodic capacity as a function of $\bar{\lambda}_c$.

6. Conclusions

The future of vehicular networks will probably be driven by increasing demand for capacity for safety and entertainment applications. The next evolutionary step in this direction is to enable V2V communication at 28 GHz. Thus, in this work, the interference analysis of vehicular networks has been performed for the 28 GHz band for V2V communications. We have derived closed-form expressions of PEP and ergodic capacity and validated them by performing extensive simulations. The diversity analysis shows that PEP depends on the number of multipath clusters and channel non-linearity. This work presents guidelines for quantifying the PEP and ergodic capacity of V2V communication at 28 GHz.

In the future, we aim to look at the integration of sub-6-GHz and mmWave for efficient vehicular communications. In this context, it would be interesting to quantify the impact of channel uncertainties on V2V communications. We anticipate that in the presence of incomplete knowledge of the channel, the performance of vehicular networks would degrade resulting in higher values of PEP. These challenging yet interesting studies would probably be conducted in the future.

Abbreviations

The following abbreviations are used in this manuscript:

PEP	Packet error probability
LOS	Line-of-sight
V2X	Vehicle-to-everything
BS	Base station
ICI	Inter-carrier-interference
SNR	Signal-to-noise ratio
FCC	Federal Communications Commission
RSU	Road side unit
AWGN	Additive white Gaussian noise
CH	Cluster head
CDF	Cumulative distribution function
PDF	Probability density function
ETSI	European Telecommunications Standards Institute
V2I	Vehicle-to-infrastructure
MIMO	Multiple-input multiple-output
ITS	Intelligent transportation system
mmWave	Millimeter wave
V2V	Vehicle-to-vehicle

References

1.	Jameel, F.; Chang, Z.; Huang, J.; Ristaniemi, T. Internet of Autonomous Vehicles: Architecture, Features, and Socio-Technological Challenges. *IEEE Wirel. Commun.* **2019**, *26*, 21–29. [CrossRef]

2.	Ligo, A.; Peha, J.M. Spectrum Policies for Intelligent Transportation Systems. TPRC 45: The 45th Research Conference on Communication, Information and Internet Policy 2017. Available online: https://papers.ssrn.com/sol3/papers.cfm?abstract_id=2943688 (accessed on 6 January 2020).

3.	ETSI. Intelligent Transport Systems (ITS); Access Layer Specification for Intelligent Transport Systems Operating in the 5 GHz Frequency Band; Technical Report EN 302 663; Version 1.2.0; 650 Route des Lucioles F-06921 Sophia Antipolis Cedex - FRANCE,2012. Available online: https://www.etsi.org/deliver/etsi_en/302600_302699/302663/01.02.01_30/en_302663v010201v.pdf (accessed on 6 January 2020).

4.	IEEE.802.11. IEEE Standard for Information Technology–Telecommunications and Information Exchange between Systems Local and Metropolitan Area Networks–Specific Requirements—Part 11: Wireless LAN Medium Access Control (MAC) and Physical Layer (PHY) Specifications; IEEE Std 802.11-2016 (Revision of IEEE Std 802.11-2012); IEEE Standards, USA, 2016; pp. 1–3534. doi:10.1109/IEEESTD.2016.7786995 Available online: https://ieeexplore.ieee.org/document/7786995 (accessed on 6 January 2020). [CrossRef]

5.	3GPP: Initial Cellular V2X standard completed. 3GPP News Journal, USA, 2016. Available online: https://www.3gpp.org/news-events/3gpp-news/1798-v2x_r14 (accessed on 6 January 2020).

6.	Choi, J.; Va, V.; Gonzalez-Prelcic, N.; Daniels, R.; Bhat, C.R.; Heath, R.W. Millimeter-Wave Vehicular Communication to Support Massive Automotive Sensing. *IEEE Commun. Mag.* **2016**, *54*, 160–167. doi:10.1109/MCOM.2016.1600071CM. [CrossRef]

7.	Jameel, F.; Wyne, S.; Nawaz, S.J.; Chang, Z. Propagation channels for mmWave vehicular communications: State-of-the-art and future research directions. *IEEE Wirel. Commun.* **2018**, *26*, 144–150. [CrossRef]

8.	Shimizu, T.; Va, V.; Bansal, G.; Heath, R.W. Millimeter Wave V2X Communications: Use Cases and Design Considerations of Beam Management. In Proceedings of the 2018 Asia-Pacific Microwave Conference (APMC), Kyoto, Japan, 6–9 November 2018; pp. 183–185. [CrossRef]

9.	Schafer, W. Channel modelling of short-range radio links at 60 GHz for mobile intervehicle communication. In Proceedings of the 41st IEEE Vehicular Technology Conference, St. Louis, MO, USA, 19–22 May 1991; pp. 314–319. [CrossRef]

10.	Andrisano, O.; Chiani, M.; Tralli, V.; Frullone, M.; Moss, C.R. Millimetre Wave Short Range Communications for Advanced Transport Telematics. *Eur. Trans. Telecommun.* **1993**, *4*, 403–414. [CrossRef]

11. ElHalawany, B.M.; Jameel, F.; Da Costa, D.B.; Dias, U.S.; Wu, K. Performance Analysis of Downlink NOMA Systems over κ-μ Shadowed Fading Channels. *IEEE Trans. Veh. Technol.* **2019**, *69*, 1046–1050. [CrossRef]

12. Anwar, W.; Franchi, N.; Fettweis, G. Performance Evaluation of Next Generation V2X Communication Technologies: 5G NR-V2V vs. IEEE 802.11bd. In Proceedings of the IEEE 90th Vehicular Technology Conference (VTC-Fall 2019), At Honolulu, HI, USA, 22–25 September 2019.

13. Magueta, R.; Teodoro, S.; Castanheira, D.; Silva, A.; Dinis, R.; Gameiro, A. Multiuser Equalizer for Hybrid Massive MIMO mmWave CE-OFDM Systems. *Appl. Sci.* **2019**, *9*, 3363. [CrossRef]

14. Magueta, R.; Castanheira, D.; Silva, A.; Dinis, R.; Gameiro, A. Hybrid multi-user equalizer for massive MIMO millimeter-wave dynamic subconnected architecture. *IEEE Access* **2019**, *7*, 79017–79029. [CrossRef]

15. Castanheira, D.; Lopes, P.; Silva, A.; Gameiro, A. Hybrid beamforming designs for massive MIMO millimeter-wave heterogeneous systems. *IEEE Access* **2017**, *5*, 21806–21817. [CrossRef]

16. Magueta, R.; Castanheira, D.; Silva, A.; Dinis, R.; Gameiro, A. Hybrid iterative space-time equalization for multi-user mmW massive MIMO systems. *IEEE Trans. Commun.* **2016**, *65*, 608–620. [CrossRef]

17. Jameel, F.; Haider, M.A.A.; Butt, A.A.. Second order fading statistics of UAV networks. In Proceedings of the 2017 Fifth International Conference on Aerospace Science & Engineering (ICASE), Islamabad, Pakistan, 14–16 November 2017; pp. 1–6.

18. Jameel, F.; Jabeen, F.; Hamid, Z. Analysis of co-channel interference in VANETs under nakagami-m fading. In Proceedings of the 2016 International Conference on Frontiers of Information Technology (FIT), Islamabad, Pakistan, 19–21 December 2016; pp. 153–158.

19. Khan, F.; Pi, Z. mmWave mobile broadband (MMB): Unleashing the 3–300 GHz spectrum. In Proceedings of the 34th IEEE Sarnoff Symposium, Princeton, NJ, USA, 3–4 May 2011; pp. 1–6. [CrossRef]

20. Jameel, F.; Haider, M.A.A.; Butt, A.A. Robust localization in wireless sensor networks using RSSI. In Proceedings of the 2017 13th International Conference on Emerging Technologies (ICET), Islamabad, Pakistan, 27–28 December 2017; pp. 1–6.

21. Giordani, M.; Mezzavilla, M.; Dhananjay, A.; Rangan, S.; Zorzi, M. Channel Dynamics and SNR Tracking in Millimeter Wave Cellular Systems. In Proceedings of the 22th European Wireless Conference, VDE Association, Oulu, Finland, 18–20 May 2016; pp. 306–313. Available online: https://arxiv.org/abs/1604.05623 (accessed on 6 January 2020)

22. Verdone, R. Outage probability analysis for short-range communication systems at 60 GHz in ATT urban environments. *IEEE Trans. Veh. Technol.* **1997**, *46*, 1027–1039. [CrossRef]

23. Wang, Y.; Venugopal, K.; Heath, R.W.; Molisch, A.F. MmWave vehicle-to-infrastructure communication: Analysis of urban microcellular networks. *IEEE Trans. Veh. Technol.* **2018**, [CrossRef]

24. Petrov, V.; Kokkoniemi, J.; Moltchanov, D.; Lehtomaki, J.; Juntti, M.; Koucheryavy, Y. The Impact of Interference From the Side Lanes on mmWave/THz Band V2V Communication Systems with Directional Antennas. *IEEE Trans. Veh. Technol.* **2018**, *67*, 5028–5041. [CrossRef]

25. Giordani, M.; Rebato, M.; Zanella, A.; Zorzi, M. Coverage and connectivity analysis of millimeter wave vehicular networks. *Ad Hoc Netw.* **2018**, *80*, 158–171. [CrossRef]

26. Bazzi, A.; Masini, B.; Zanella, A.; Thibault, I. On the performance of IEEE 802.11p and LTE-V2V for the Cooperative Awareness of Connected Vehicles. *IEEE Trans. Veh. Technol.* **2017**, *66*, 10419–10432. [CrossRef]

27. Bazzi, A.; Masini, B.M.; Zanella, A. How many vehicles in the LTE-V2V awareness range with half or full duplex radios? In Proceedings of the 2017 15th International Conference on ITS Telecommunications (ITST), Warsaw, Poland, 29–31 May 2017; pp. 1–6. [CrossRef]

28. Anwar, W.; Kulkarni, K.; Augustin, T.R.; Franchi, N.; Fettweis, G. PHY Abstraction Techniques for IEEE 802.11p and LTE-V2V: Applications and Analysis. In Proceedings of the 2018 IEEE Global Communications Conference, Abu Dhabi, UAE, 9–13 December 2018; pp. 1–7.

29. Chen, J.; Mao, G.; Li, C.; Zafar, A.; Zomaya, A.Y. Throughput of Infrastructure-Based Cooperative Vehicular Networks. *IEEE Trans. Intell. Transp. Syst.* **2017**, *18*, 2964–2979. [CrossRef]

30. Rappaport, T.S.; Sun, S.; Mayzus, R.; Zhao, H.; Azar, Y.; Wang, K.; Wong, G.N.; Schulz, J.K.; Samimi, M.; Gutierrez, F. Millimeter Wave Mobile Communications for 5G Cellular: It Will Work! *IEEE Access* **2013**, *1*, 335–349. [CrossRef]

31. Bai, T.; Alkhateeb, A.; Heath, R.W. Coverage and capacity of millimeter-wave cellular networks. *IEEE Commun. Mag.* **2014**, *52*, 70–77. [CrossRef]

32. Wang, H.; Liu, R.P.; Ni, W.; Chen, W.; Collings, I.B. VANET Modeling and Clustering Design Under Practical Traffic, Channel and Mobility Conditions. *IEEE Trans. Commun.* **2015**, *63*, 870–881. [CrossRef]

33. Jameel, F.; Khan, F.; Haider, M.A.A.; Haq, A.U. On physical layer security of two way energy harvesting relays. In Proceedings of the 2017 International Conference on Frontiers of Information Technology (FIT), Islamabad, Pakistan, 18–20 December 2017; pp. 35–40.

34. Dos Anjos, A.A.; Marins, T.R.R.; de Souza, R.A.A.; Yacoub, M.D. Higher Order Statistics for the $\alpha - \eta - \kappa - \mu$ Fading Model. *IEEE Trans. Antennas Propag.* **2018**, *66*, 3002–3016. [CrossRef]

35. Yacoub, M.D. The $\alpha - \eta - \kappa - \mu$ Fading Model. *IEEE Trans. Antennas Propag.* **2016**, *64*, 3597–3610. [CrossRef]

36. Gradshteyn, I.S.; Ryzhik, I.M. *Table of Integrals, Series, and Products*; Academic Press: New York, NY, USA, 2014.

37. Brychkov, Y.A.; Marichev, O.; Prudnikov, A. *Integrals and Series, Vol. 3: More Special Functions*; Gordon and Breach Science Publishers: Amsterdam, The Netherlands, 1990.

38. Ansari, I.S.; Abdallah, M.M.; Alouini, M.S.; Qaraqe, K.A. Outage performance analysis of underlay cognitive RF and FSO wireless channels. In Proceedings of the 2014 3rd International Workshop in Optical Wireless Communications (IWOW), Funchal, Portugal, 17 September 2014; pp. 6–10.